Structural Evolution of Crystalline Conjugated Polymer/Fullerene Domains from Solution to the Solid State in the Presence and Absence of an Additive

ARTICLE *in* THE JOURNAL OF PHYSICAL CHEMISTRY C · JANUARY 2015

Impact Factor: 4.77

8 AUTHORS, INCLUDING:

Cheng-Si Tsao

Institute of Nuclear Energy Research

41 PUBLICATIONS **703** CITATIONS

SEE PROFILE

Hou-Chin Cha

Institute of Nuclear Energy Research

25 PUBLICATIONS **254** CITATIONS

SEE PROFILE

Kung-Hwa Wei

National Chiao Tung University

172 PUBLICATIONS **6,230** CITATIONS

SEE PROFILE

THE JOURNAL OF PHYSICAL CHEMISTRY C

Article

pubs.acs.org/JPCC

Structural Evolution of Crystalline Conjugated Polymer/Fullerene Domains from Solution to the Solid State in the Presence and Absence of an Additive

Yu-Wei Su,[†] Chih-Ming Liu,[†] Jian-Ming Jiang,[†] Cheng-Si Tsao,*[,‡] Hou-Chin Cha,[‡] U-Ser Jeng,[§] Hsing-Lung Chen,[∥] and Kung-Hwa Wei*[,†]

[†]Department of Materials Science and Engineering, National Chiao Tung University, 1001 Ta Hsueh Road, Hsinchu 30050, Taiwan

[‡]Institute of Nuclear Energy Research, 1000 Wen-Hua Road, Longtan, Taoyuan 32546, Taiwan

[§]National Synchrotron Radiation Center, 101 Hsin-Ann Road, Hsinchu 30077, Taiwan

[∥]Department of Chemical Engineering, National Tsing Hua University, 101 Section 2, Kuang-Fu Road, Hsinchu 30013, Taiwan

Supporting Information

ABSTRACT: The power conversion efficiencies of polymer/fullerene solar cells are critically dependent on the nanometer-scale morphologies of their active layers, which are typically processed from solution. Using synchrotron wide- and small-angle X-ray scattering, we have elucidated the intricate mechanism of the structural transitions from solutions to solid films of the crystalline polymer poly[bis(dodecyl)thiophene-thieno[3,4-*c*]pyrrole-4,6-dione] (PBTTPD) and [6,6]-phenyl-C_{71}-butyric acid methyl ester ($PC_{71}BM$), including the effect of the solvent additive 1,6-diiodohexane (DIH). We found that the local assembly of rigid-rod PBTTPD segments that formed in solution instantly and then relaxed within several hundred seconds upon cooling to room temperature from 90 °C could re-emerge and develop into seeds for subsequent crystallization of the polymer in the solid films. At room temperature (25 °C), the presence of DIH in chlorobenzene slightly enhanced the formation of local assembly PBTTPD segments in the supersaturated PBTTPD in PBTTPD/$PC_{71}BM$ blend solution. Two cases of films were subsequently developed from these blend solutions with drop-casted and spin-coated methods. For spin-coated thin films (90 nm thick), which evolve quickly, polymer's crystallinity and the fullerene packing in the solid-state thin films were enhanced in the case of involving DIH. Regarding the effect of DIH for processing the drop-casted thick films (2.5 μm thick), which evolve slowly, DIH has no observable effect on PBTTPD/$PC_{71}BM$ structure. Our results provide some understanding of the mechanism behind the structural development of polymer/fullerene blends upon their transitions from solution to the solid state, as well as the key functions of the additive.

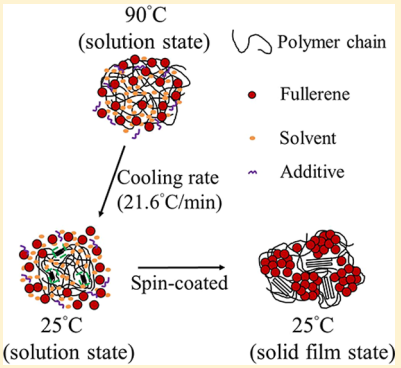

INTRODUCTION

With the development of new polymers, device architectures, and processing methods, bulk heterojunction (BHJ) solar cells,[1,2] which feature active layers comprising polymers as the electron donors and fullerenes as the electron acceptors, have achieved high photon-to-electron power conversion efficiencies (PCEs; ca. 11%).[3] Several studies have revealed that the PCE of a BHJ solar cell is critically not only dependent on the molecular weight[4,5] and trace impurities[6] of polymers, but also on the nanometer-scale morphology[7−12] of its thin active layer, which is typically spin-coated from solution. For optimized device performance, the active layer usually has a thickness of between 100 and 300 nm; it comprises intricate hierarchical structures of three phases: phase-separated polymer domains, aggregated fullerene domains, as well as molecularly intermixed polymer/fullerene domains.[13−15] All types of structures in the active layer play important roles toward obtaining devices with high photocurrents: the molecularly intermixed domains of fullerene molecules and polymer chains provide interfaces for efficient charge transfer and dissociation of photogenerated excitons, while the phase-separated polymer and fullerene domains form effective percolation pathways for the transport of dissociated holes and electrons, respectively, to their respective electrodes. The morphology of the active layer in a BHJ solar cell can be optimized by tuning the chemical composition, the solvent used for film casting, the postprocessing treatment (e.g., thermal or solvent annealing),[16−18] and the additives used (if any).[19,20]

At present, our knowledge of the structures of polymer/fullerene blends in solution[21] is not at such a level that we can always process them into solid films in an optimized manner. Although the study of the effect of additives and solvent drying[22] on the overall phase diagrams of P3HT/fullerene[23] has been undertaken, only a few reports[24−27] have concerned the

Received: December 10, 2014
Revised: January 13, 2015
Published: January 16, 2015

DOI: 10.1021/jp512315a
J. Phys. Chem. C 2015, 119, 3408−3417

structural evolution of crystalline medium-band gap polymers, which usually provide higher photovoltaic performance, and fullerenes in solution, as well as their subsequent structural transitions to solid films. Because the final morphology of the active layer evolves from the morphology of its components in solution (sometimes in the presence of additive) and depends critically on the processing method, if we are to further enhance device performance it is imperative that we decipher the structures of these polymers and fullerenes in solution and track their evolution to the solid state so that we can tune the active layer morphology.

Small-angle X-ray scattering (SAXS) is a powerful tool for probing nanostructures having dimensions ranging from 1 to 100 nm.[28−30] It provides ensemble-averaged details regarding the internal structures of the polymer/fullerene thin films[31,32] as well as the capacity for time-resolved in situ analysis of structural evolution and the kinetics of such transformations.[25,26,33−36] Grazing-incidence wide-angle X-ray scattering (GIWAXS)[23,37−39] and grazing-incidence small-angle X-ray scattering (GISAXS) techniques have been particularly useful for quantitative structural analyses of thin films to determine their degrees of polymer crystallization[26,27,40−43]and fullerene aggregation, and to infer their mutual influence on multiple length scales.[44]

Recently, SAXS has been used to probe the structures of conjugated polymer solutions, in particular to identify interchain aggregation in these solutions with respect to concentration and solvent quality,[45−49] and to examine the effects of additives on the aggregation of the polymer and fullerene.[21] Moreover, the structures of conjugated polymers presenting various alkyl side chains,[50] solvent-induced nucleation,[51] and the rates of polymer aggregation[52] have all been characterized using this scattering technique. The link between the structures of polymer/fullerene blends in solution and those formed subsequently in the solid state has, however, been studied only rarely. It is important to establish this connection because the onset of crystallization of the conjugated polymer, the evolution of the polymer conformation, and fullerene aggregation upon proceeding from solution to the solid film all determine the final morphology of the active layer. This relevant knowledge can provide viable strategies in designing and fabricating bulk heterojunction photovoltaics with suitable processing methods, ultimately leading to high PCEs.

We first employed SAXS to study the temperature-dependent and kinetic behavior of the disorder-to-order transition (DOT) of the polymer's conformation in solution. We then investigated the structures of a crystalline conjugated polymer, a fullerene, and their blends in various solutions and monitored their transitions from solution to the solid state using in situ X-ray scattering,[53] in the presence of additive, to decipher the mechanism of crystallization.

In this study, we hypothesized that the incorporation of an additive in the polymer/fullerene blend solutions promotes the onset of the formation of ordered domains of a crystalline conjugate polymer upon cooling, due to the higher solubility of the fullerene than that of the polymer in the additive. We expect that the structure of the solid film precipitated from the blend solution will be determined by a combination of the initial structure in the solution state, in the presence or absence of the additive, and the subsequent kinetic effect involved in the transition from the solution to the solid state.

Figure 1 shows the molecular structures of poly[bis-(dodecyl)thiophene-thieno[3,4-*c*]pyrrole-4,6-dione] (PBTTPD),[54] [6,6]-phenyl-C_{71}-butyric acid methyl ester ($PC_{71}BM$) as our blends and 1,6-diiodohexane (DIH) as a solvent additive. We have demonstrated the device PCEs of PBTTPD/$PC_{71}BM$ greater than 7% using chloroform (CF) as the solvent.[41] Our aim was to elucidate the mechanisms behind the various transformations and the function of the additive to provide critical knowledge for improving the processing and performance of future devices.

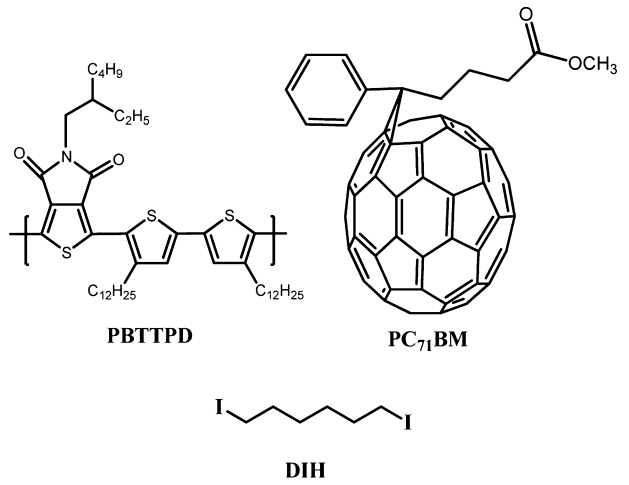

Figure 1. Molecular structures of the polymer PBTTPD, the fullerene $PC_{71}BM$, and the solvent additive DIH.

EXPERIMENTAL METHODS

Solutions of PBTTPD and $PC_{71}BM$ in anhydrous chlorobenzene (CB: Sigma-Aldrich) were prepared in a glovebox (dry N_2: <1 ppm of O_2, <1 ppm of H_2O) by dissolving PBTTPD (M_n = 11.7 kg/mol; PDI = 1.4) and $PC_{71}BM$ (Sigma-Aldrich, >99%) individually at concentrations of 6 and 9 mg/mL (0.6 and 0.9 wt %), respectively. All sample solutions were not prepared under the deaeration process. The reason we chose CB as the solvent for PBTTPD instead of CF is that CF can lead to a high scattering intensity background, which obscures the scattering from the polymer or fullerene. Subsequently, the blend solution was prepared by dissolving PBTTPD (6 mg) and $PC_{71}BM$ (9 mg) together in anhydrous CB (1 mL). DIH, the solvent additive, was added to the PBTTPD, $PC_{71}BM$, and blend solutions at a concentration of 0.5 vol % (1 μL:200 μL). The blend ratio for PBTTPD/$PC_{71}BM$ (1/1.5 by weight) and the amount of the additive were chosen on the basis of the device that contained the optimized active layer that produced high PCEs as reported in our previous studies.[41,54] All solutions were stirred at 90 °C for 6 h to dissolve all of the ingredients. Table 1 shows the solubility of PBTTPD and $PC_{71}BM$ in CB and DIH at room temperature, respectively, determined using the modified solubility test[55] of ASTM E1148.

SAXS measurements were performed using the BL23A beamline of the National Synchrotron Radiation Research Center (NSRRC), Taiwan. All SAXS samples were prepared in the form of liquids, encapsulated with a stainless-steel cell (diameter, 4 mm; thickness, 1.8 mm for empty volume) featuring a quartz window. SAXS measurements of all of the well-sealed solutions were conducted under a temperature-programmed controlled environment in the transmission mode,

DOI: 10.1021/jp512315a
J. Phys. Chem. C 2015, 119, 3408−3417

Table 1. Solubility of PBTTPD and $PC_{71}BM$ in CB and DIH, Respectively, at Room Temperature Using a Modified Solubility Test[55] of ASTM E1148

solvent	PBTTPD (mg/mL)	$PC_{71}BM$ (mg/mL)
CB (bp = 132 °C)	2.2	21.1
DIH (bp = 282 °C)	1.6	21.0

using a collimated beam having energy of 14 keV. The SAXS profile was also measured for the cell containing purely the solvent CB. All SAXS scattering profiles, $I(q)$, were measured on an absolute intensity scale, with the scattering vector defined as $q = (1/\lambda)4\pi \sin(\theta/2)$ in terms of the scattering angle (θ) and the X-ray wavelength (λ). During the SAXS measurements, for each data point, we moved the sample holder around for four measurements; after the first SAXS measurement, we moved the sample holder 2 mm horizontally for the second measurement, then 2 mm vertically for the third measurement, and last 2 mm horizontally for the fourth measurement forming a square beam-irradiated enclosed region within the cell with a diameter of 4 mm. Each measurement lasts only around 1s. The averaged value obtained from these four measurements was recorded as one data point. Thus, there is no part of solution measured under the continuous synchrotron irradiation; the possibility of the irradiation damage on the samples is very low. The SAXS measurements of the $PC_{71}BM$, PBTTPD, and blend (PBTTPD/$PC_{71}BM$) solutions, with and without additive, were performed over three consecutive steps: (1) at 90 °C, (2) while cooling from 90 to 25 °C (cooling rate: 21.6 °C/min), and (3) at 25 °C. In situ SAXS measurements (time frame: 10 s) were conducted for steps (2) and (3) to determine the evolution of the temperature-dependent SAXS profiles (normalized to the cooling rate) during cooling and of the time-resolved SAXS profiles during the period of 30 min at 25 °C. The standard deviations of the collected SAXS data were typically within 1%; the standard deviations of the SAXS profiles in the high-q region were between 5% and 8%. The standard deviations decreased significantly upon increasing the SAXS intensities.

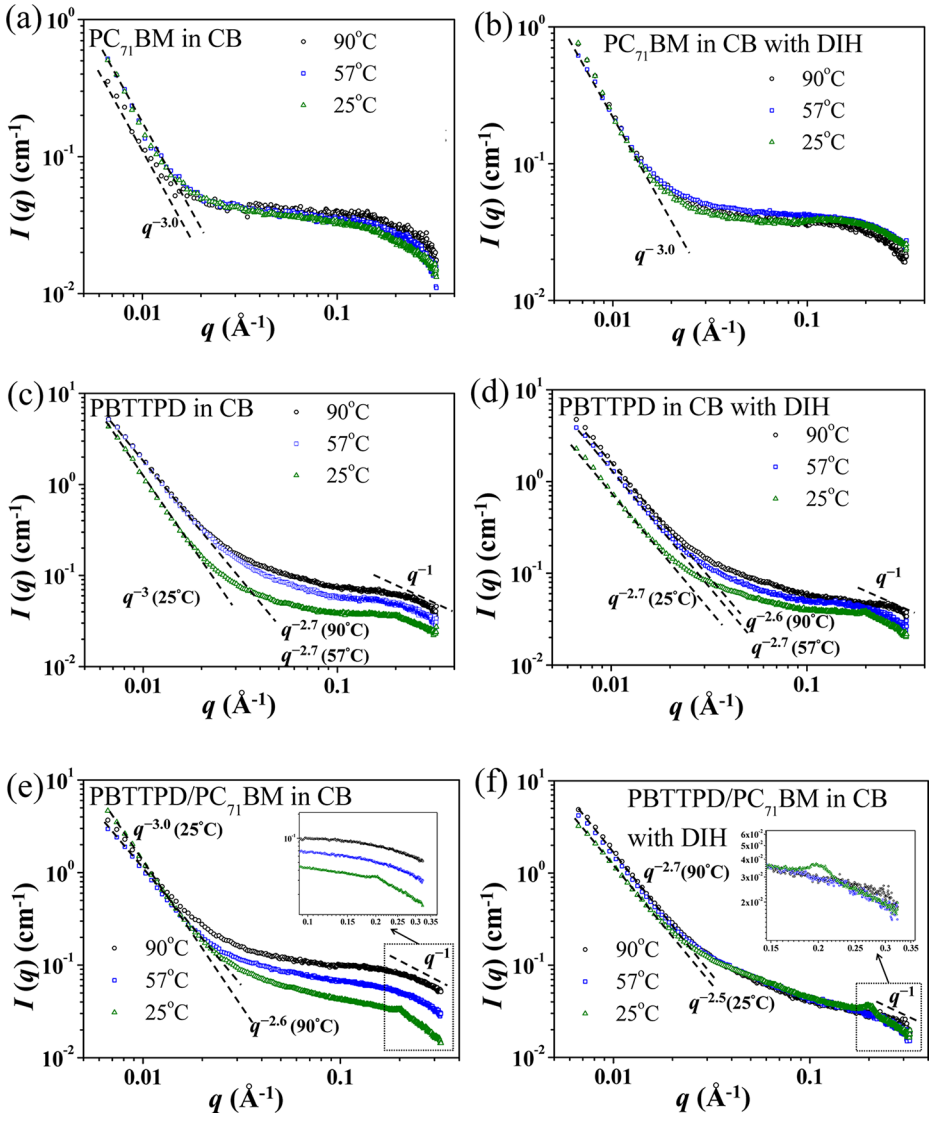

Figure 2. SAXS profiles of CB solutions of (a) 9 mg/mL $PC_{71}BM$, (b) 9 mg/mL $PC_{71}BM$ with 0.5 vol % DIH, (c) 6 mg/mL PBTTPD, (d) 6 mg/mL PBTTPD with 0.5 vol % DIH, (e) 15 mg/mL PBTTPD/$PC_{71}BM$ (1:1.5, w/w), and (f) 15 mg/mL PBTTPD/$PC_{71}BM$ (1:1.5, w/w) with 0.5 vol % DIH.

DOI: 10.1021/jp512315a
J. Phys. Chem. C 2015, 119, 3408−3417

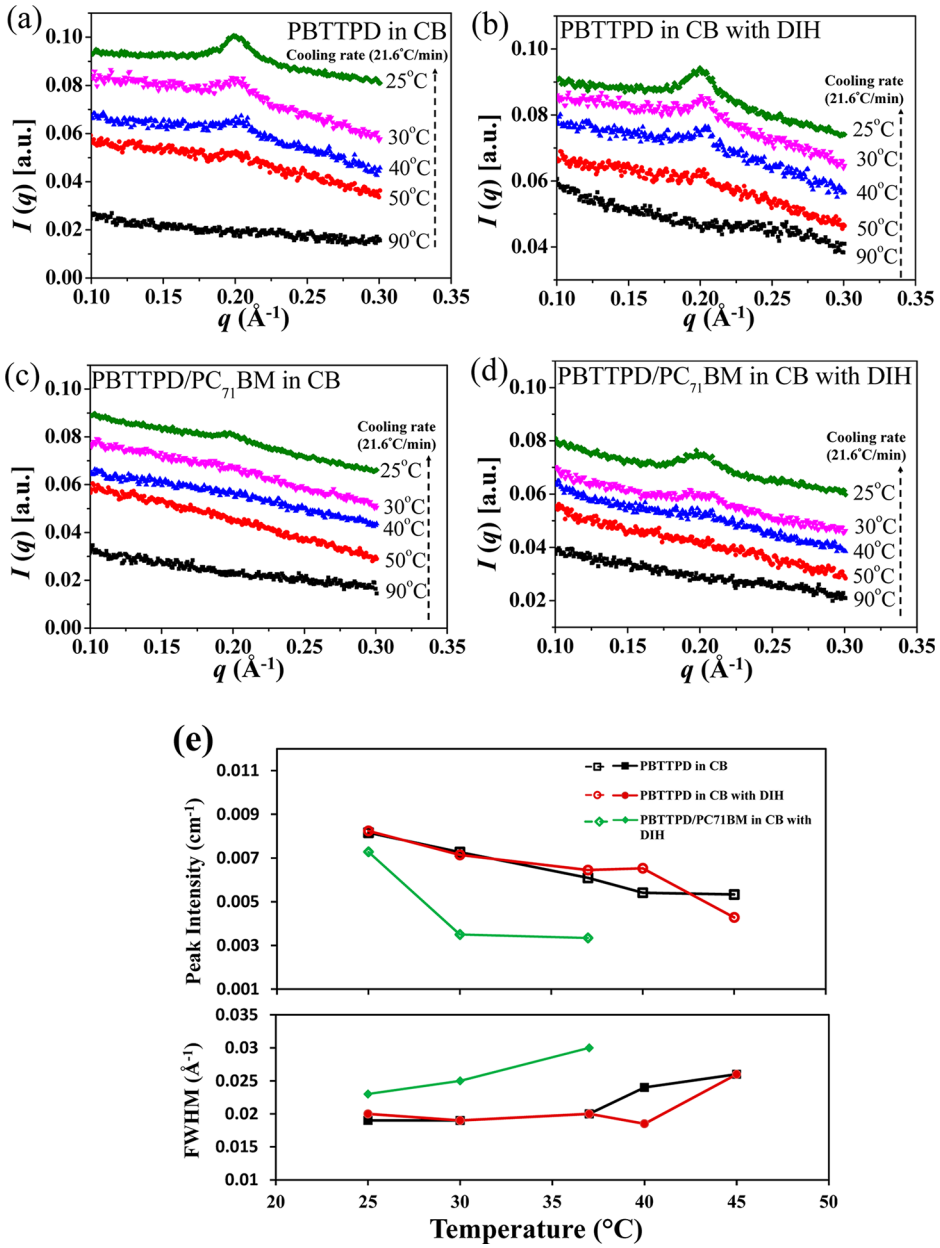

Figure 3. (a–d) Temperature-dependent SAXS profiles in the high-q region of CB solutions of (a) 6 mg/mL PBTTPD, (b) 6 mg/mL PBTTPD with 0.5 vol % DIH, (c) 15 mg/mL PBTTPD/$PC_{71}BM$ (1:1.5, w/w), and (d) 15 mg/mL PBTTPD/$PC_{71}BM$ (1:1.5, w/w) with 0.5 vol % DIH. (e) fwhm and intensity of the peak at a value of q of 0.2 $Å^{-1}$, plotted with respect to temperature.

To further investigate the morphological evolution from the solution to crystallization in the film, in situ GIWAXS (BL23A beamline, NSRRC) was performed (grazing angle: 0.2°) after drop-casted and spin-coated samples of blend solutions onto silicon wafers that contained a deposited layer of poly(3,4-ethylenedioxythiophene)-polystyrenesulfonate (PEDOT:PSS). These samples were prepared in the same manner as those used for the SAXS measurements. The drop-casted sample was placed in a chamber equipped with a hose connected to a vacuum pump to control the rate of solvent evaporation. The GIWAXS profile was recorded as a function of time at ambient pressure and then under low vacuum to evaporate the solvent completely. The radiation exposure time (including sample alignment) for drop-casted film for each measurement lasted for 15 min of. After that, the beam was blanked for 15 min of nonexposure time and then was ready for the next radiation exposure measurement. The spin-coated film samples were prepared under the condition of spinning the substrate at 1500 rpm for 60 s and then placed in a N_2-filled glovebox for drying 12 h prior to measurement. The thickness of the drop-casted films that had experienced ambient annealing for 180 min and the thickness of the spin-coated films that had experienced ambient annealing for 12 h were 2.5 μm and 100 nm, respectively, as measured using a surface profilometer (Veeco Dektak 150).

RESULTS AND DISCUSSION

Figure 2 presents the temperature-dependent SAXS profiles of solutions of $PC_{71}BM$ (9 mg/mL), PBTTPD (6 mg/mL), and 15 mg/mL PBTTPD/$PC_{71}BM$ (1:1.5, w/w) in CB, with or without DIH. The profile of pure solvent (CB) was obtained first and was shown in Figure S1 (Supporting Information).

DOI: 10.1021/jp512315a
J. Phys. Chem. C 2015, 119, 3408–3417

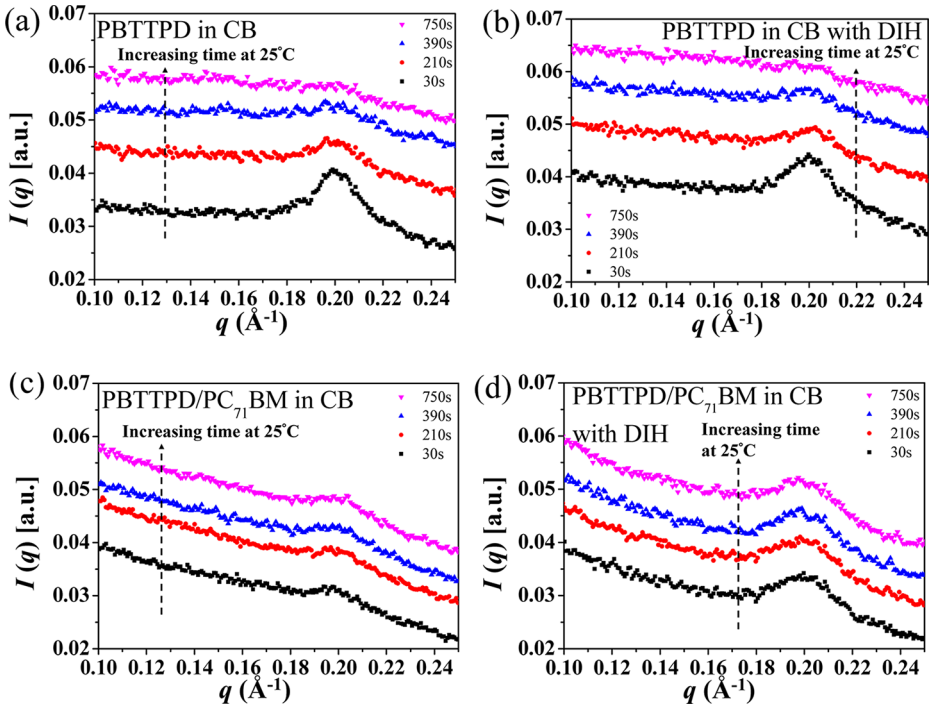

Figure 4. Time-resolved SAXS profiles at 25 °C in the high-q region of CB solutions of (a) 6 mg/mL PBTTPD, (b) 6 mg/mL PBTTPD with 0.5 vol % DIH, (c) 15 mg/mL PBTTPD/$PC_{71}BM$, and (d) 15 mg/mL PBTTPD/$PC_{71}BM$ with 0.5% DIH.

The SAXS profiles of the 9 mg/mL $PC_{71}BM$ solution [Figure 2a] revealed a power-law dependence of the scattering intensity $I(q)$ on the scattering vector q [i.e., $I(q) \propto q^{-3}$] in the low-q region (0.006 $Å^{-1} < q < 0.03$ $Å^{-1}$), indicating the formation of a large aggregate structure with the characteristic fractal dimension of 3. A shoulder (a typical form factor profile) appeared in the high-q region (0.3 $Å^{-1} > q > 0.1$ $Å^{-1}$), implying the existence of individually dispersed $PC_{71}BM$ molecules. Hence, large $PC_{71}BM$ agglomerate and individually dispersed $PC_{71}BM$ molecules coexisted in the solution at temperatures ranging from 25 to 90 °C. The scattering profiles of the 9 mg/mL $PC_{71}BM$ solution containing 0.5 vol % DIH [Figure 2b] exhibited almost the same shape as those of the pristine $PC_{71}BM$ solution, indicating that DIH had essentially no effect on the behavior of $PC_{71}BM$ in solution at low concentration.

The profile of the pristine PBTTPD solution [Figure 2c] also revealed a power-law dependence [$I(q) \propto q^{-n}$] in both the low- and the high-q regions. The scattering features attested that the large-scale aggregates of PBTTPD chains adopted a fractal network structure, with fractal dimensions of 2.7, 2.7, and 3 at 90, 57, and 25 °C, respectively. The increase in the fractal dimension upon decreasing the temperature indicates that the network became more compact at lower temperature as a result of poorer solvent solubility. In particular, the upturns at the low-q region of the SAXS profiles imply that relatively large PBTTPD domain sizes dominated in the pristine PBTTPD solutions. On the other hand, the scattering intensities of the PBTTPD solutions in the high-q region ($q > 0.2$ $Å^{-1}$) displayed the power-law dependence of $I(q) \propto q^{-1}$, indicating that the chain segments constructing the network adopted rigid rod conformations[49,50] regardless of the temperature. After addition of DIH into the polymer solution, Figure 2d reveals only slight changes in the SAXS profiles (with a slightly less steep slope in low-q region at 25 °C), while the profiles at other temperatures were similar to those of the pristine PBTTPD solution. Figure 2e and f displays the SAXS profiles of the 15 mg/mL PBTTPD/$PC_{71}BM$ (1:1.5, w/w) blend solutions in the absence and presence of DIH, respectively. A comparison of the SAXS profiles of PBTTPD/$PC_{71}BM$ [Figure 2e] with those of the PBTTPD solution [Figure 2c] indicates that the addition of $PC_{71}BM$ to the PBTTPD solution led to the appearance of a weak structural peak at a value of q of 0.2 $Å^{-1}$ at 25 °C. We attribute this peak to the local assembly of PBTTPD segments that yielded ordered nanodomains in the solution. Moreover, a comparison of Figure 2e with f reveals that the presence of DIH in the blend solution resulted in a slightly stronger intensity of the peak at 0.2 $Å^{-1}$ at 25 °C, implying slightly enhanced local assembly of the chain segments in the PBTTPD/$PC_{71}BM$ blend solution. Figure 2a–d reveals that the SAXS intensities of the pure polymer solution were 1 order magnitude higher than those of the pure $PC_{71}BM$, implying that the SAXS profiles of the blend solutions reflect the structure of the polymer more than that of $PC_{71}BM$ in solution. To identify the nature of the peak at 0.2 $Å^{-1}$, we conducted more detailed time- and temperature-dependent SAXS studies (see below).

Disorder-to-Order Transition (DOT) Temperatures of Local Segmental Assemblies in Solution. Figure 3 presents the temperature-dependent SAXS profiles of the solutions of 6 mg/mL PBTTPD and 15 mg/mL PBTTPD/$PC_{71}BM$ (1:1.5, w/w) blend, both with and without DIH upon cooling from 90 to 25 °C. In Figure 3a and b, we observe that a weak peak appeared at a value of q of 0.2 $Å^{-1}$ and that it grew progressively as the temperature decreased from 90 to 25 °C, indicating the development of local segmental assembly of PBTTPD in solution. When DIH was present, the intensity of this peak was slightly enhanced; that is, a small content of DIH could slightly enhance the segmental assembly. On the other hand, Figure 3a and c reveals that the addition of $PC_{71}BM$ to the solutions caused the intensity of the peak at 0.2 $Å^{-1}$ to decrease, presumably because the $PC_{71}BM$ molecules incorporated into

DOI: 10.1021/jp512315a
J. Phys. Chem. C 2015, 119, 3408–3417

the polymer chains hampered the segmental assembly during the cooling process. The addition of DIH to the PBTTPD/$PC_{71}BM$ blend solutions increased the intensity of the signal at 0.2 $Å^{-1}$ slightly at 25 °C, relative to that of the pristine PBTTPD/$PC_{71}BM$ blend solution [Figure 3d]. We suspect that the presence of DIH could promote the local segmental assembly of PBTTPD due to the low solubility of PBTTPD in DIH, as shown in Table 1.

We used the full-width-at-half-maximum (FWHM) of the scattering peak at 0.2 $Å^{-1}$ as an indicator of the size distribution of the ordered nanodomains formed by the polymer segments.[56] Figure 3e presents the FWHMs and the peak intensities for the different solutions plotted with respect to the temperature during the cooling process; the peak intensity increased and the corresponding FWHMs decreased upon decreasing the temperature from 50 to 25 °C. The peak intensity of the 15 mg/mL PBTTPD/$PC_{71}BM$ blend solutions incorporating DIH was slightly higher than that of the pristine blend solutions (i.e., absence of DIH). A dramatic decrease in the FWHM or a large increase in the corresponding peak intensity occurred during the cooling of these solutions, indicating a transition from a disordered phase to a locally ordered phase for the segments; therefore, we could determine the disorder-to-order transition temperatures (T_{DOT}) of these solutions from the plots of fwhm or peak intensity with respect to temperature.[56] The value of T_{DOT} was approximately 47 °C for the 6 mg/mL PBTTPD solution in either the absence or the presence of DIH (0.5 vol %). Upon the addition of 9 mg/mL $PC_{71}BM$ into the polymer solutions, the value of T_{DOT} decreased to 39 °C for the PBTTPD/$PC_{71}BM$ blend solution and to 27 °C for the PBTTPD/$PC_{71}BM$ solution containing DIH, indicating that the bulkiness of the $PC_{71}BM$ clusters retarded the formation of ordered nanodomains from the PBTTPD segments.

To examine the stability of the ordered nanodomains of PBTTPD segments, we performed time-resolved SAXS analyses on the solutions. Figure 4a–d displays the time-resolved SAXS profiles in the high-q region of solutions of PBTTPD, PBTTPD incorporating DIH, PBTTPD/$PC_{71}BM$, and PBTTPD/$PC_{71}BM$ incorporating DIH, respectively, immediately after cooling to 25 °C. Interestingly, the peak at 0.2 $Å^{-1}$ for the pristine PBTTPD solution diminished over time at 25 °C, almost disappearing after 750 s [Figure 4a]. This observation revealed that the ordered segmental assembly was kinetic, rather than thermodynamic, in nature; the polymer segmental ordering formed first, due to some local segmental interactions, but the ordered nanodomains relaxed as the polymer network structure subsequently reorganized. Given enough time, the polymers formed a thermodynamically stable state in which the polymers crystallize from the solution because the concentration of the polymers is much larger than its solubility in CB at 25 °C. The behavior of the PBTTPD solution containing DIH [Figure 4b] was almost the same as that of the pristine PBTTPD solution, albeit with a slower pace of relaxation of the ordered nanodomains. In the presence of $PC_{71}BM$ [Figure 4c and d], however, the peak at 0.2 $Å^{-1}$ remained essentially unperturbed over time at 25 °C, indicating that $PC_{71}BM$ tended to retard the kinetics of the local segmental assembly, and also hindered the relaxation of the ordered domains.

Figure 5 shows schematic representations of the formation and subsequent relaxation of the segmental ordering and network reorganization of PBTTPD in its pristine and blend

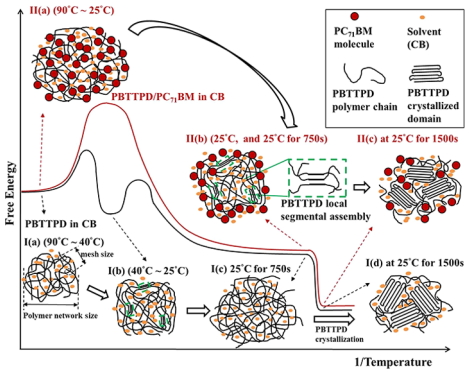

Figure 5. Schematic representation of the evolution of polymer local segmental assembly, with and without depicting the surrounding $PC_{71}BM$ domains, for 6 mg/mL PBTTPD and 15 mg/mL PBTTPD/$PC_{71}BM$ solutions cooling from 90 to 25 °C.

solutions on a hierarchy of length scales in terms of free energy. The PBTTPD polymer network structure in the solution can be characterized by two length scales: global length scale and local mesh size. At the global length scale, the polymer network structure started to reorganize toward an equilibrium state (i.e., the more compact network) during the cooling from 90 °C [I(a) in Figure 5], which requires a certain diffusion time associated with such a global structure reorganization. At the local length scale, the polymer segments around the overlap points/regions in the network with higher concentration than elsewhere in the solution may form ordered nanodomains rapidly because of their spatial proximity upon cooling below the value of T_{DOT} [I(b) in Figure 5]. The characteristic time scale associated with such a segmental assembling process is significantly shorter than that for the overall polymer network reorganization. The formation of the ordered nanodomains lowered the energy of the system, thereby bringing the solution to a local free energy minimum corresponding to a metastable equilibrium state. Nevertheless, the tendency of the polymer system to reach the global free energy minimum resulted in subsequent reorganization of the network structure to a more compact network form. This progress relaxed the originally formed ordered nanodomains at 25 °C after 750 s [I(c) in Figure 5]. Consequently, the network structure reorganization of PBTTPD in solution upon cooling can be envisioned to occur through two steps in its kinetic pathway: (1) the formation of ordered nanodomains, which led to the first stage of compaction of the network, and (2) further reorganization of the network to reach its equilibrium compact form, which invariably relaxed the ordered nanodomains. In the presence of $PC_{71}BM$ [II(a) in Figure 5], local segmental assembly may also occur at temperatures below the value of T_{DOT}, but the global reorganization of the network structure was strongly hampered by the $PC_{71}BM$ molecules for some time. The network compaction process would probably eventually result in the rejection of some $PC_{71}BM$ molecules from polymer networks that are more than their thermodynamic equilibrium amount in the well-mixed PBTTPD/fullerene domain, which involves another high activation barrier or much longer time scale. Therefore, the ordered nanodomains remained after prolonged storage at 25 °C, as illustrated in II(b) in Figure 5.

Although the formation of ordered nanodomains through assembly of local polymer segments was kinetic in origin, their existence over a certain period of time might have great implications for structural development in the solid thin film, a

DOI: 10.1021/jp512315a
J. Phys. Chem. C 2015, 119, 3408–3417

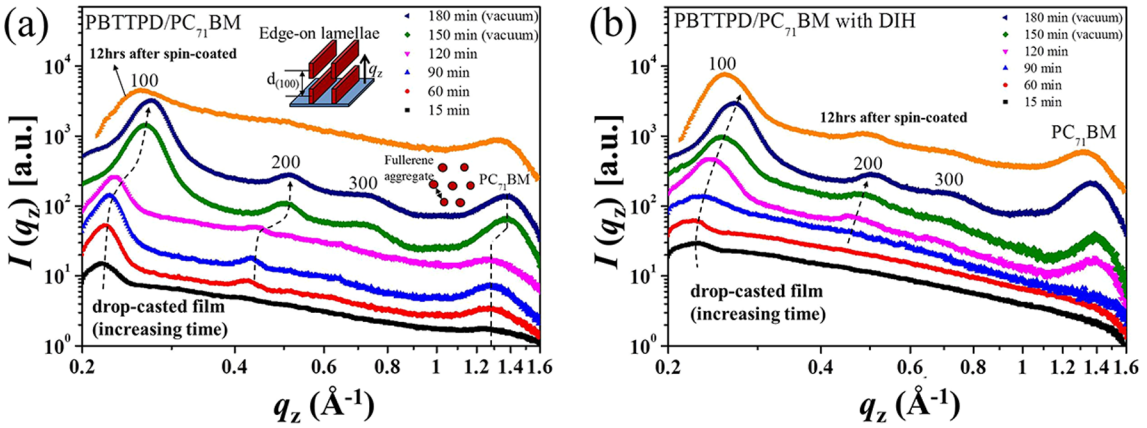

Figure 6. Time-resolved out-of-plane GIWAXS profiles of the drop-cast 15 mg/mL PBTTPD/$PC_{71}BM$ (1:1.5, w/w) blend in CB solution in the (a) absence and (b) presence of 0.5 vol % DIH, from solution to the solid film state, as compared to the profiles of the spin-coated film.

typical active layer in photovoltaic devices, because the time scale for processing is usually much shorter than that for polymers to reach their equilibrium state. On the basis of the Ostwald rule, crystallization from solutions often starts in a thermodynamically unstable phase and is followed by recrystallization to a thermodynamically stable phase.[57] In our case, the local segmental assembly of PBTTPD that appeared instantly upon quenching the solution (from 90 °C) to 25 °C but disappeared after 750 s represents a thermodynamically unstable phase; once the PBTTPD solution remains at 25 °C for more than 1500 s, PBTTPD solution will develop nucleating seeds for subsequent recrystallization [I(d) in Figure 5] because the concentration of PBTTPD solution is over its solubility in CB at 25 °C. The sequence of these events, therefore, is consistent with the Ostwald rule given enough time. We have thus determined that the ordered domains (local segmental assembly) in the solution could re-emerge and form the nucleating seeds for subsequent recrystallization of the polymer in solid polymer films when the solvent and additive had all evaporated, a phenomenon that had been speculated previously.[24] In the presence of $PC_{71}BM$, PBTTPD solution develops nucleation seeds for subsequent crystallization [II(c) in Figure 5] without going through the recrystallization process as in the case of PBTTPD solution [I(d) in Figure 5].

Structural Evolution of Polymers from Blend Solutions to Thin Films upon Drop-Casted or Spin-Coated. To understand the effect of the rate of solvent removal on the structural evolution of the polymer (Supporting Information Figure S2) and fullerene to their final solid state, we performed time-resolved analyses of samples prepared through casting the PBTTPD/$PC_{71}BM$ blend solutions upon drop-casted and spin-coated. Figure 6a and b presents the evolution of the out-of-plane GIWAXS profiles of the PBTTPD/$PC_{71}BM$ blend solutions that had been dropped and spun onto substrates in the absence and presence of 0.5 vol % DIH, respectively, at 90 °C, with the scattering background of a PEDOT:PSS-coated silicon wafer being deducted from the data. Figure 6a reveals that the (100) reflection peak at a value of q_z of 0.22 $Å^{-1}$ emerged for the PBTTPD solution after it had been dropped onto a substrate for 15 min in a chamber under an ambient environment, suggesting that the ordered nanodomains (contributing to the peak at 0.2 $Å^{-1}$) in solution might have formed the seeds for crystallization. The position of this (100) peak shifted gradually to 0.22, 0.23, and 0.24 $Å^{-1}$ after 60, 90, and 120 min, respectively. After 150 min, we applied air suction to the chamber to accelerate the solvent evaporation; the (100) peak then shifted from 0.26 to 0.27 $Å^{-1}$ at 180 min, indicating that the *d*-spacing of the edge-on PBTTPD lamellae decreased from 29 to 23 Å as the crystalline structure became consolidated during the solvent evaporation process. The (200) and (300) peaks appeared after 60 and 150 min, respectively. The (200) peak shifted from 0.42 $Å^{-1}$ after 60 min to 0.51 $Å^{-1}$ after 150 min, while the (300) peak was located at 0.74 $Å^{-1}$ after 150 min.

The values of q_z for the halo in the high-q_z region changed from 1.28 to 1.39 $Å^{-1}$ after 60 and 150 min, revealing that the intermolecular distance between the two $PC_{71}BM$ molecules decreased as the solvent evaporated. The final thickness of the drop-casted film was approximately 2.5 μm. In contrast, the spin-coated thin film (thickness: 90 nm) displayed only the weak (100) peak of PBTTPD after 12 h in glovebox because the solvent has been cast off the surface during solution spinning, implying that the polymer crystallinity was influenced significantly by the kinetics of the film formation process. That is, the drop-casted process and the spin-coated process allow slow and rapid removal of the solvent, respectively, resulting in long and short durations for polymer crystallization and also thick and thin films.

In the presence of DIH [Figure 6b], the (100) peak appeared initially at a value of q_z of 0.23 $Å^{-1}$ after 90 min, and gradually moved to 0.24, 0.25, and 0.27 $Å^{-1}$ after 120, 150, and 180 min, respectively. The (200) and (300) reflection peaks did not appear until 120 and 180 min, respectively. The (200) peak shifted from 0.49 to 0.5 $Å^{-1}$. The $PC_{71}BM$ halo located at a value of q_z of 1.39 $Å^{-1}$ after 120 min; it remained unchanged until 180 min. The crystallization (100) and (200) peaks for the spin-coated film were located at the same values of q_z as those of the drop-casted film after 150 min. For the drop-casted film, the addition of DIH did not have a significant effect in the final state that was dried for 180 min because the slow evaporation of the solvent for the thicker films allowed more time for crystallization of the PBTTPD polymer and packing of the fullerene molecules in both the control sample and the solution containing DIH.

In the spin-coated case, the addition of DIH had a significant effect because thin films required less time to reach complete solvent removal. The film formation process influenced the polymer crystallinity when using either the drop-casted or the spin-coated method. Our findings support the hypothesis that an early local ordered structure that yields a peak at q of 0.2 $Å^{-1}$

DOI: 10.1021/jp512315a
J. Phys. Chem. C 2015, 119, 3408−3417

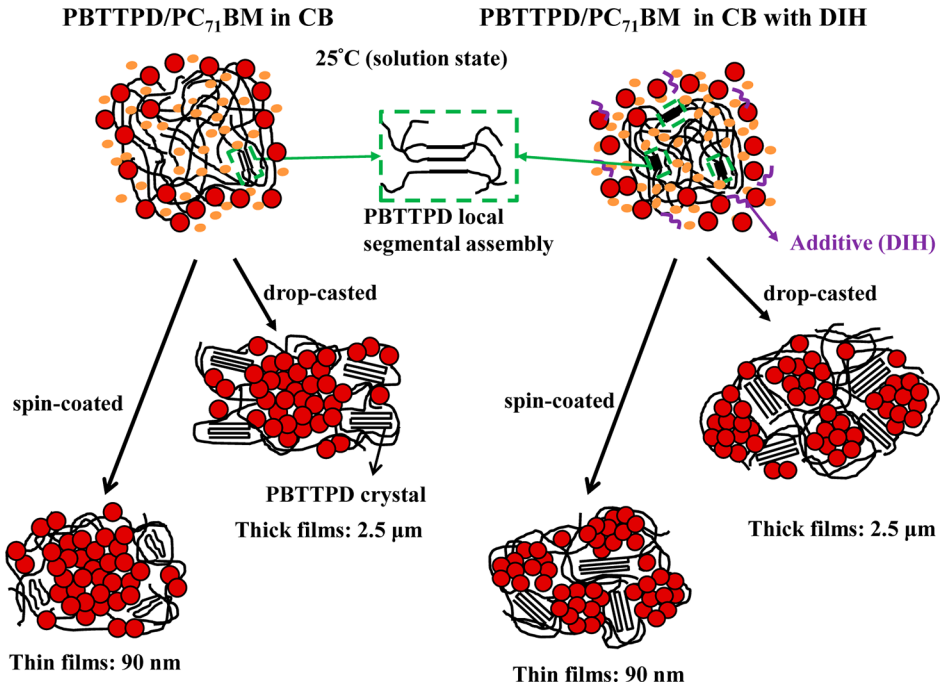

Figure 7. Schematic representations of the structural evolution of 15 mg/mL PBTTPD/$PC_{71}BM$ blend solutions, in the absence and presence of DIH, from solution at 25 °C to the solid film state, upon applying different deposition processes.

exists in the PBTTPD or blend solutions during the solvent cooling process; this signal developed into the (100) peak at a value of q_z of 0.23 $Å^{-1}$ for the PBTTPD lamellae after 90 min in the drop-casted system.

Figure 7 displays a schematic representation of the structural evolution from the PBTTPD/$PC_{71}BM$ blend solutions at 25 °C to their solid films after drop-casted and spin-coated for 12 h. The presence of DIH has no significant effect on the crystallinity of PBTTPD for the drop-casted thick films, but could lead to a substantial enhancement for the spin-coated thin films. DIH could promote the onset of the local segmental assembly of PBTTPD in the blend solution, but whether DIH can affect the polymer crystallinity of the solid films will depend on the film thickness or the removal speed of DIH (i.e., drop-casted versus spin-coated). It takes a much longer time for the drop-casted film of 2.5 μm to have the CB solvent completely removed than for the spin-coated film of 90 nm, and thus allows more time for the polymer to crystallize more completely for the drop-casted case. The incorporation of DIH leads to smaller $PC_{71}BM$ agglomerates in the final solid films, as inferred from the solution scattering data.

CONCLUSION

In solution, the evolution of the local segmental assembly of the conjugated chains of the polymer PBTTPD depends on the temperature, time (a kinetic process), and nature of the additive, if any. In the presence of $PC_{71}BM$, local polymer chain ordering became less sensitive to time and temperature because of the bulkiness of the $PC_{71}BM$ domains. The segmental assembly of rigid-rod polymers occurred in solution at temperatures below the disorder-to-order transition temperature, first appearing and then disappearing, and can re-emerge and develop into the seeds for subsequent crystallization of the polymer in the presence of fullerenes in solid films as the solvent evaporated. In the presence of the additive DIH, the local assembly of PBTTPD segments is not significantly affected by DIH, consistent with the observation that the relative solubility of the PBTTPD in DIH is similar to that in CB. At room temperature (25 °C), DIH slightly enhanced the supersaturated PBTTPD in PBTTPD/$PC_{71}BM$ blend solution to form local assembly PBTTPD segments. In the kinetically controlled transitions from the PBTTPD/$PC_{71}BM$ blends in solution to the solid state, the additive DIH plays a more critical role in enhancing both the crystallinity of the polymer and the intermolecular packing of the fullerene when the rate of solvent removal is much higher, such as in the case of a spin-coated process relative to that of a drop-casted process. These results provide greater fundamental understanding of the structural development of polymer/fullerene blends in solution upon cooling to form solid active layers, as well as the molecular function and kinetic nature of the additive.

ASSOCIATED CONTENT

Supporting Information

SAXS scattering profiles of pure CB, $PC_{71}BM$ in CB, and PBTTPD in CB solutions. Time-resolved out-of-plane GIWAXS profiles of the PBTTPD in CB solution from solution to the solid film state. Detailed procedure of the solubility test. This material is available free of charge via the Internet at http://pubs.acs.org.

AUTHOR INFORMATION

Corresponding Authors

*Tel.: (886) 3-471-1400, ext 6427. E-mail: cstsao@iner.gov.tw.
*Tel.: (886) 3-573-1871. E-mail: khwei@mail.nctu.edu.tw.

Notes

The authors declare no competing financial interest.

ACKNOWLEDGMENTS

This project is funded by the National Science Council, Taiwan (NSC 98-2120-M-009-006). We thank Dr. Chun-Jen Su for his

DOI: 10.1021/jp512315a
J. Phys. Chem. C 2015, 119, 3408−3417

assistance in operating the wide/small-angle X-ray scattering facility.

REFERENCES

(1) Yu, G.; Gao, J.; Hummelen, J. C.; Wudl, F.; Heeger, A. J. Polymer Photovoltaic Cells: Enhanced Efficiencies via a Network of Internal Donor-Acceptor Heterojunctions. *Science* **1995**, *270*, 1789−1791.
(2) Darling, S. B.; You, F. Q. The Case for Organic Photovoltaics. *RSC Adv.* **2013**, *3*, 17633−17648.
(3) You, J.; Dou, L.; Yoshimura, K.; Kato, T.; Ohya, K.; Moriarty, T.; Emery, K.; Chen, C.-C.; Gao, J.; Li, G.; et al. A Polymer Tandem Solar Cell with 10.6% Power Conversion Efficiency. *Nat. Commun.* **2013**, *4*, 1446.
(4) Li, W.; Yang, L.; Tumbleston, J. R.; Yan, L.; Ade, H.; You, W. Controlling Molecular Weight of a High Efficiency Donor-Acceptor Conjugated Polymer and Understanding Its Significant Impact on Photovoltaic Properties. *Adv. Mater.* **2014**, *26*, 4456−4462.
(5) Bartelt, J. A.; Douglas, J. D.; Mateker, W. R.; Labban, A. E.; Tassone, C. J.; Toney, M. F.; Fréchet, J. M. J.; Beaujuge, P. M.; McGehee, M. D. Controlling Solution-Phase Polymer Aggregation with Molecular Weight and Solvent Additives to Optimize Polymer-Fullerene Bulk Heterojunction Solar Cells. *Adv. Energy Mater.* **2014**, *4*, 1301733.
(6) Nikiforov, M. P.; Lai, B.; Chen, W.; Chen, S.; Schaller, R. D.; Strzalka, J.; Maser, J.; Darling, S. B. Detection and Role of Trace Impurities in High-Performance Organic Solar Cells. *Energy Environ. Sci.* **2013**, *6*, 1513−1520.
(7) Yang, X.; Loos, J.; Veenstra, S. C.; Verhees, W. J. H.; Wienk, M. M.; Kroon, J. M.; Michels, M. A. J.; Janssen, R. A. J. Nanoscale Morphology of High-Performance Polymer Solar Cells. *Nano Lett.* **2005**, *5*, 579−583.
(8) Yao, Y.; Hou, J. H.; Xu, Z.; Li, G.; Yang, Y. Effect of Solvent Mixture on the Nanoscale Phase Separation in Polymer Solar Cells. *Adv. Funct. Mater.* **2008**, *18*, 1783−1789.
(9) Ma, W.; Yang, C.; Gong, X.; Lee, K.; Heeger, A. J. Thermally Stable, Efficient Polymer Solar Cells with Nanoscale Control of the Interpenetrating Network Morphology. *Adv. Funct. Mater.* **2005**, *15*, 1617−1622.
(10) Liao, H.-C.; Ho, C.-C.; Chang, C.-Y.; Jao, M.-H.; Darling, S. B.; Su, W.-F. Additives for Morphology Control in High-Efficiency Organic Solar Cells. *Mater. Today* **2013**, *16*, 326−336.
(11) Ruderer, M. A.; Müller-Buschbaum, P. Morphology of Polymer-Based Bulk Heterojunction Films for Organic Photovoltaics. *Soft Matter* **2011**, *7*, 5482−5493.
(12) Hains, A. W.; Ramanan, C.; Irwin, M. D.; Liu, J.; Wasielewski, M. R.; Marks, T. J. Designed Bithiophene-Based Interfacial Layer for High-Efficiency Bulk-Heterojunction Organic Photovoltaic Cells. Importance of Interfacial Energy Level Matching. *ACS Appl. Mater. Interfaces* **2010**, *2*, 175−185.
(13) Treat, N. D.; Varotto, A.; Takacs, C. J.; Batara, N.; Al-Hashimi, M.; Heeney, M. J.; Heeger, A. J.; Wudl, F.; Hawker, C. J.; Chabinyc, M. L. Polymer-Fullerene Miscibility: A Metric for Screening New Materials for High-Performance Organic Solar Cells. *J. Am. Chem. Soc.* **2012**, *134*, 15869−15879.
(14) Westacott, P.; Tumbleston, J. R.; Shoaee, S.; Fearn, S.; Bannock, J. H.; Gilchrist, J. B.; Heutz, S.; DeMello, J.; Heeney, M.; Ade, H.; et al. On the Role of Intermixed Phases in Organic Photovoltaic Blends. *Energy Environ. Sci.* **2013**, *6*, 2756−2764.
(15) Chen, C.-Y.; Tsao, C.-S.; Huang, Y.-C.; Liu, H.-W.; Chiu, W.-Y.; Chuang, C.-M.; Jeng, U.-S.; Su, C.-J.; Wu, W.-R.; Su, W.-F.; et al. Mechanism and Control of the Structural Evolution of a Polymer Solar Cell from a Bulk Heterojunction to a Thermally Unstable Hierarchical Structure. *Nanoscale* **2013**, *5*, 7629−7638.
(16) Su, Y.-W.; Lan, S.-C.; Wei, K.-H. Organic Photovoltaics. *Mater. Today* **2012**, *15*, 554−562.
(17) Chen, H.; Hu, S.; Zang, H.; Hu, B.; Dadmun, M. Precise Structural Development and its Correlation to Function in Conjugated Polymer: Fullerene Thin Films by Controlled Solvent Annealing. *Adv. Funct. Mater.* **2013**, *23*, 1701−1710.
(18) Bartelt, J. A.; Beiley, Z. M.; Hoke, E. T.; Mateker, W. R.; Douglas, J. D.; Collins, B. A.; Tumbleston, J. R.; Graham, K. R.; Amassian, A.; Ade, H.; et al. The Importance of Fullerene Percolation in the Mixed Regions of Polymer−Fullerene Bulk Heterojunction Solar Cells. *Adv. Energy Mater.* **2013**, *3*, 364−374.
(19) Lee, J. K.; Ma, W. L.; Brabec, C. J.; Yuen, J.; Moon, J. S.; Kim, J. Y.; Lee, K.; Bazan, G. C.; Heeger, A. J. Processing Additives for Improved Efficiency from Bulk Heterojunction Solar Cells. *J. Am. Chem. Soc.* **2008**, *130*, 3619−3623.
(20) Etzold, F.; Howard, I. A.; Forler, N.; Cho, D. M.; Meister, M.; Mangold, H.; Shu, J.; Hansen, M. R.; Müllen, K.; Laquai, F. The Effect of Solvent Additives on Morphology and Excited-State Dynamics in PCPDTBT:PCBM Photovoltaic Blends. *J. Am. Chem. Soc.* **2012**, *134*, 10569−10583.
(21) Lou, S. J.; Szarko, J. M.; Xu, T.; Yu, L. P.; Marks, T. J.; Chen, L. X. Effects of Additives on the Morphology of Solution Phase Aggregates Formed by Active Layer Components of High-Efficiency Organic Solar Cells. *J. Am. Chem. Soc.* **2011**, *133*, 20661−20663.
(22) Shin, N.; Richter, L. J.; Herzing, A. A.; Kline, R. J.; DeLongchamp, D. M. Effect of Processing Additives on the Solidification of Blade-Coated Polymer/Fullerene Blend Films via In-Situ Structure Measurements. *Adv. Energy Mater.* **2013**, *3*, 938−948.
(23) Schmidt-Hansberg, B.; Sanyal, M.; Klein, M. F. G.; Pfaff, M.; Schnabel, N.; Jaiser, S.; Vorobiev, A.; Müller, E.; Colsmann, A.; Scharfer, P.; et al. Moving through the Phase Diagram: Morphology Formation in Solution Cast Polymer−Fullerene Blend Films for Organic Solar Cells. *ACS Nano* **2011**, *5*, 8579−8590.
(24) Schmidt, K.; Tassone, C. J.; Niskala, J. R.; Yiu, A. T.; Lee, O. P.; Weiss, T. M.; Wang, C.; Fréchet, J. M. J.; Beaujuge, P. M.; Toney, M. F. A Mechanistic Understanding of Processing Additive-Induced Efficiency Enhancement in Bulk Heterojunction Organic Solar Cells. *Adv. Mater.* **2014**, *26*, 300−305.
(25) Liu, F.; Gu, Y.; Wang, C.; Zhao, W.; Chen, D.; Briseno, A. L.; Russell, T. P. Efficient Polymer Solar Cells Based on a Low Bandgap Semi-crystalline DPP Polymer-PCBM Blends. *Adv. Mater.* **2012**, *24*, 3947−3951.
(26) Rogers, J. T.; Schmidt, K.; Toney, M. F.; Bazan, G. C.; Kramer, E. J. Time-Resolved Structural Evolution of Additive-Processed Bulk Heterojunction Solar Cells. *J. Am. Chem. Soc.* **2012**, *134*, 2884−2887.
(27) Gu, Y.; Wang, C.; Russell, T. P. Multi-Length-Scale Morphologies in PCPDTBT/PCBM Bulk-Heterojunction Solar Cells. *Adv. Energy Mater.* **2012**, *2*, 683−690.
(28) Kewalramani, S.; Zwanikken, J. W.; Macfarlane, R. J.; Leung, C.-Y.; Olvera de la Cruz, M.; Mirkin, C. A.; Bedzyk, M. J. Counterion Distribution Surrounding Spherical Nucleic Acid−Au Nanoparticle Conjugates Probed by Small-Angle X-ray Scattering. *ACS Nano* **2013**, *7*, 11301−11309.
(29) Chen, W.; Nikiforov, M. P.; Darling, S. B. Morphology Characterization in Organic and Hybrid Solar Cells. *Energy Environ. Sci.* **2012**, *5*, 8045−8074.
(30) Chen, C.-M.; Huang, Y.-J.; Wei, K.-H. Structural Development of Gold and Silver Nanoparticles within Hexagonally Ordered Spherical Micellar Diblock Copolymer Thin Films. *Nanoscale* **2014**, *6*, 5999−6008.
(31) Chiu, M.-Y.; Jeng, U.-S.; Su, C.-H.; Liang, K. S.; Wei, K.-H. Simultaneous Use of Small- and Wide-Angle X-ray Techniques to Analyze Nanometerscale Phase Separation in Polymer Heterojunction Solar Cells. *Adv. Mater.* **2008**, *20*, 2573−2578.
(32) Kozub, D. R.; Vakhshouri, K.; Orme, L. M.; Wang, C.; Hexemer, A.; Gomez, E. D. Polymer Crystallization of Partially Miscible Polythiophene/Fullerene Mixtures Controls Morphology. *Macromolecules* **2011**, *44*, 5722−5726.
(33) Wu, W.-R.; Jeng, U.-S.; Su, C.-J.; Wei, K.-H.; Su, M.-S.; Chiu, M.-Y.; Chen, C.-Y.; Su, W.-B.; Su, C.-H.; Su, A.-C. Competition between Fullerene Aggregation and Poly(3-hexylthiophene) Crystallization upon Annealing of Bulk Heterojunction Solar Cells. *ACS Nano* **2011**, *5*, 6233−6243.
(34) Verploegen, E.; Miller, C. E.; Schmidt, K.; Bao, Z. N.; Toney, M. F. Manipulating the Morphology of P3HT-PCBM Bulk Hetero-

DOI: 10.1021/jp512315a
J. Phys. Chem. C 2015, 119, 3408−3417

junction Blends with Solvent Vapor Annealing. *Chem. Mater.* **2012**, *24*, 3923−3931.
(35) Chou, K. W.; Yan, B. Y.; Li, R. P.; Li, E. Q.; Zhao, K.; Anjum, D. H.; Alvarez, S.; Gassaway, R.; Biocca, A.; Thoroddsen, S. T.; et al. Spin-Cast Bulk Heterojunction Solar Cells: A Dynamical Investigation. *Adv. Mater.* **2013**, *25*, 1923−1929.
(36) Lu, H. Y.; Akgun, B.; Russell, T. P. Morphological Characterization of a Low-Bandgap Crystalline Polymer:PCBM Bulk Heterojunction Solar Cells. *Adv. Energy Mater.* **2011**, *1*, 870−878.
(37) Sirringhaus, H.; Brown, P. J.; Friend, R. H.; Nielsen, M. M.; Bechgaard, K.; Langeveld-Voss, B. M. W.; Spiering, A. J. H.; Janssen, R. A. J.; Meijer, E. W.; Herwig, P.; et al. Two-Dimensional Charge Transport in Self-Organized, High-Mobility Conjugated Polymers. *Nature* **1999**, *401*, 685−688.
(38) Li, G.; Yao, Y.; Yang, H.; Shrotriya, V.; Yang, G.; Yang, Y. "Solvent Annealing" Effect in Polymer Solar Cells Based on Poly(3-hexylthiophene) and Methanofullerenes. *Adv. Funct. Mater.* **2007**, *17*, 1636−1644.
(39) Chen, D.; Nakahara, A.; Wei, D. G.; Nordlund, D.; Russell, T. P. P3HT/PCBM Bulk Heterojunction Organic Photovoltaics: Correlating Efficiency and Morphology. *Nano Lett.* **2011**, *11*, 561−567.
(40) Chen, W.; Xu, T.; He, F.; Wang, W.; Wang, C.; Strzalka, J.; Liu, Y.; Wen, J. G.; Miller, D. J.; Chen, J. H.; et al. Hierarchical Nanomorphologies Promote Exciton Dissociation in Polymer/Fullerene Bulk Heterojunction Solar Cells. *Nano Lett.* **2011**, *11*, 3707−3713.
(41) Su, M.-S.; Kuo, C.-Y.; Yuan, M.-C.; Jeng, U.-S.; Su, C.-J.; Wei, K.-H. Improving Device Efficiency of Polymer/Fullerene Bulk Heterojunction Solar Cells Through Enhanced Crystallinity and Reduced Grain Boundaries Induced by Solvent Additives. *Adv. Mater.* **2011**, *23*, 3315−3319.
(42) Liu, C.-M.; Su, M.-S.; Jiang, J.-M.; Su, Y.-W.; Su, C.-J.; Chen, C.-Y.; Tsao, C.-S.; Wei, K.-H. Distribution of Crystalline Polymer and Fullerene Clusters in Both Horizontal and Vertical Directions of High-Efficiency Bulk Heterojunction Solar Cells. *ACS Appl. Mater. Interfaces* **2013**, *5*, 5413−5422.
(43) Liu, C.-M.; Su, Y.-W.; Jiang, J.-M.; Chen, H.-C.; Lin, S.-W.; Su, C.-J.; Jeng, U.-S.; Wei, K.-H. Complementary Solvent Additives Tune the Orientation of Polymer Lamellae, Reduce the Sizes of Aggregated Fullerene Domains, and Enhance the Performance of Bulk Heterojunction Solar Cells. *J. Mater. Chem. A* **2014**, *2*, 20760−20769.
(44) Liao, H.-C.; Tsao, C.-S.; Lin, T.-H.; Chuang, C.-M.; Chen, C.-Y.; Jeng, U.-S.; Su, C.-H.; Chen, Y.-F.; Su, W.-F. Quantitative Nanoorganized Structural Evolution for a High Efficiency Bulk Heterojunction Polymer Solar Cell. *J. Am. Chem. Soc.* **2011**, *133*, 13064−13073.
(45) Li, Y.-C.; Chen, K.-B.; Chen, H.-L.; Hsu, C.-S.; Tsao, C.-S.; Chen, J.-H.; Chen, S.-A. Fractal Aggregates of Conjugated Polymer in Solution State. *Langmuir* **2006**, *22*, 11009−11015.
(46) Ou-Yang, W.-C.; Chang, C.-S.; Chen, H.-L.; Tsao, C.-S.; Peng, K.-Y.; Chen, S.-A.; Han, C. C. Micellelike Aggregates in Solutions of Semirigid Hairy-Rod Polymers. *Phys. Rev. E* **2005**, *72*, 031802.
(47) Burrows, H. D.; Tapia, M. J.; Fonseca, S. M.; Valente, A. J. M.; Lobo, V. M. M.; Justino, L. L. G.; Qiu, S.; Pradhan, S.; Scherf, U.; Chattopadhyay, N.; et al. Aqueous Solution Behavior of Anionic Fluorene-co-thiophene-Based Conjugated Polyelectrolytes. *ACS Appl. Mater. Interfaces* **2009**, *1*, 864−874.
(48) Choudhury, P. K.; Bagchi, D.; Menon, R. π-Conjugation and Conformation in a Semiconducting Polymer: Small Angle X-Ray Scattering Study. *J. Phys: Condens. Matter* **2009**, *21*, 195801.
(49) Choudhury, P. K.; Bagchi, D.; Sangeeth, C. S. S.; Menon, R. Modified Conformation and Physical Properties in Conducting Polymers Due to Varying Conjugation and Solvent Interactions. *J. Mater. Chem.* **2011**, *21*, 1607−1604.
(50) McCulloch, B.; Ho, V.; Hoarfrost, M.; Stanley, C.; Do, C.; Heller, W. T.; Segalman, R. A. Polymer Chain Shape of Poly(3-alkylthiophenes) in Solution Using Small-Angle Neutron Scattering. *Macromolecules* **2013**, *46*, 1899−1907.
(51) Keum, J. K.; Xiao, K.; Ivanov, I. N.; Hong, K.; Browning, J. F.; Smith, G. S.; Shao, M.; Littrell, K. C.; Rondinone, A. J.; Andrew Payzant, E.; et al. Solvent Quality-Induced Nucleation and Growth of Parallelepiped Nanorods in Dilute Poly(3-hexylthiophene) (P3HT) Solution and the Impact on the Crystalline Morphology of Solution-Cast Thin Film. *CrystEngComm* **2013**, *15*, 1114−1124.
(52) Sobkowicz, M. J.; Jones, R. L.; Kline, R. J.; DeLongchamp, D. M. Effect of Fullerenes on Crystallization-Induced Aggregation in Polymer Photovoltaics Casting Solutions. *Macromolecules* **2012**, *45*, 1046−1055.
(53) Pearson, A. J.; Wang, T.; Dunbar, A. D. F.; Yi, H.; Watters, D. C.; Coles, D. M.; Staniec, P. A.; Iraqi, A.; Jones, R. A. L.; Lidzey, D. G. Morphology Development in Amorphous Polymer:Fullerene Photovoltaic Blend Films During Solution Casting. *Adv. Funct. Mater.* **2014**, *24*, 659−667.
(54) Yuan, M.-C.; Chiu, M.-Y.; Liu, S.-P.; Chen, C.-M.; Wei, K.-H. A Thieno[3,4-c]pyrrole-4,6-dione-Based Donor-Acceptor Polymer Exhibiting High Crystallinity for Photovoltaic Applications. *Macromolecules* **2010**, *43*, 6936−6938.
(55) Voroshazi, E.; Vasseur, K.; Aernouts, T.; Heremans, P.; Baumann, A.; Deibel, C.; Xue, X.; Herring, A. J.; Athans, A. J.; Lada, T. A.; et al. Novel Bis-C_{60} Derivative Compared to Other Fullerene Bis-Adducts in High Efficiency Polymer Photovoltaic Cells. *J. Mater. Chem.* **2011**, *21*, 17345−17352.
(56) Tsao, C.-S.; Chen, H.-L. Concurrent Transformation of Copolymer Domain Morphology Induced by the Order-Disorder Transition of Comb Block in Supramolecular Comb-Coil Block Copolymer. *Macromolecules* **2004**, *37*, 8984−8991.
(57) Nývlt, J. The Ostwald Rule of Stages. *Cryst. Res. Technol.* **1995**, *30*, 443−449.

NOTE ADDED AFTER ASAP PUBLICATION

Figure 5 has been updated. The revised version was re-posted on January 30, 2015.

DOI: 10.1021/jp512315a
J. Phys. Chem. C 2015, 119, 3408−3417